Geophys. J. Int. (2002) **150,** 403–414

High-resolution teleseismic tomography of upper-mantle structure using an *a priori* three-dimensional crustal model

Felix Waldhauser,* Regina Lippitsch, Edi Kissling and Jörg Ansorge

Institute of Geophysics, Swiss Federal Institute of Technology, ETH Hönggerberg, CH-8093 *Zürich, Switzerland. E-mail: kissling@tomo.ig.erdw.ethz.ch*

Accepted 2002 January 16. Received 2002 January 15; in original form 2000 July 11

SUMMARY

The effect of an *a priori* known 3-D crustal model in teleseismic tomography of upper-mantle structure is investigated. We developed a 3-D crustal *P*-wave velocity model for the greater Alpine region, encompassing the central and western Alps and the northern Apennines, to estimate the crustal contribution to teleseismic traveltimes. The model is constructed by comparative use of published information from active and passive seismic surveys. The model components are chosen to represent the present large-scale Alpine crustal structure and for their significant effect on the propagation of seismic wavefields. They are first-order structures such as the crust–mantle boundary, sedimentary basins and the high-velocity Ivrea body. Teleseismic traveltime residuals are calculated for a realistic distribution of azimuths and distances by coupling a finite-difference technique to the IASP91 traveltime tables. Residuals are produced for a synthetic upper-mantle model featuring two slab structures and the 3-D crustal model on top of it. The crustal model produces traveltime residuals in the range between −0.7 and 1.5 s that vary strongly as a function of backazimuth and epicentral distance. We find that the non-linear inversion of the synthetic residuals without correcting for the 3-D crustal structure erroneously maps the crustal anomalies into the upper mantle. Correction of the residuals for crustal structure before inversion properly recovers the synthetic slab structures placed in the upper mantle. We conclude that with the increasing amount of high-quality seismic traveltime data, correction for near-surface structure is essential for increasing resolution in tomographic images of upper-mantle structure.

Key words: crustal structure, seismic resolution, seismic tomography, seismic-wave propagation, upper mantle.

1 INTRODUCTION

Resolution in teleseismic tomography of upper-mantle structure depends critically on our understanding of the 3-D crustal velocity structure beneath a receiver array. Because of the low frequencies and near-vertical angle of incidence of incoming waves, teleseismic traveltime tomography resolves the crustal-scale structure poorly, though complex crustal structures influence teleseismic traveltimes strongly (Baer 1980; Guyoton 1991; Weber 1994; Waldhauser 1996). When propagating through regions with a rough topography of the crust–mantle boundary and with strong intracrustal velocity inhomogeneities, teleseismic wave fronts undergo distortions that lead to significant traveltime and amplitude anomalies observed at the Earth's surface. The location and size of such traveltime anomalies depend on the lateral variation of the velocity structure, and on the backazimuth and slowness of the incoming teleseismic wave fronts. Neglecting these crustal effects in tomographic studies may significantly decrease the resolution of deeper structure, or even cause these effects to be erroneously projected into the resulting mantle structure. This is especially important for global and regional studies with the increasing higher quality of traveltime data and with high-precision teleseismic hypocentre locations (Van der Hilst *et al.* 1997; Engdahl *et al.* 1998; Bijwaard & Spakman 2000).

Whereas global crustal models have been shown to be useful in large-scale applications such as surface wave studies (Mooney *et al.* 1998), models of much higher resolution need to be developed to estimate the distortion of seismic wavefields within the crust on a regional scale, in particular in areas of complex crustal structure. Although teleseismic earthquake data can be used to determine the large-scale crustal structure (e.g. crustal thickness; Owens & Zandt 1997), and teleseismic traveltime residuals have been used to investigate the crust and upper mantle (Aki *et al.* 1977; Poupinet *et al.* 1997, among others), information from other seismic

*Now at: Lamont-Doherty Earth Observatory, Columbia University, 61 Route 9W, Palisades, NY 10964, USA. E-mail: felixw@ldeo.columbia.edu

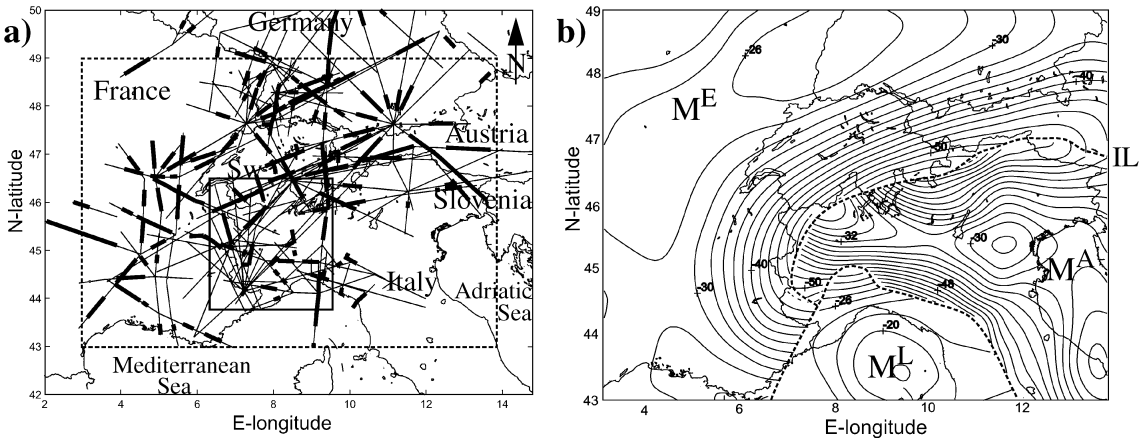

Figure 1. (a) Seismic refraction, wide-angle reflection and near-vertical reflection profiles (thin lines) carried out over the past decades in the greater Alpine region. Superimposed are published locations of 2-D-migrated Moho reflector elements (thick lines). Dashed box outlines 3-D model dimension. Solid box shows location of local earthquake tomographic model (Solarino *et al.* 1997). Sw: Switzerland. (b) Continuous Moho topography (contours at 2 km intervals) derived by 3-D modelling of 2-D near-vertical and wide-angle reflection data. The European, the Adriatic, and the Ligurian Moho interfaces are indicated (M^E, M^A, M^L, respectively). Labels attached to isolines indicate depths in km. IL: Insubric Line. Modified from Waldhauser *et al.* (1998).

methods must be exploited independently to develop a high-resolution 3-D model suitable for obtaining crustal corrections for teleseismic traveltimes before their inversion.

The Alpine region is well known for its complex 3-D crustal structure, where station corrections have been estimated to be of the order of seconds (Baer 1980; Babuska *et al.* 1990; Guyoton 1991). In the first part of this study we develop an integrated 3-D crustal *P*-velocity model encompassing the western and central Alps and the northern Apennines by combining published controlled-source seismic and local earthquake tomographic data. The model includes first-order structures such as the Moho topography, sedimentary basins and a strong intracrustal velocity anomaly known as the Ivrea body. These model components have been chosen according to their significant influence on the propagation of seismic wavefields (Baer 1980; Cattaneo & Eva 1990; Guyoton 1991).

In the second part, a synthetic data set of teleseismic traveltime residuals is generated for realistic event/station pairs and a combined mantle model with integrated synthetic slab structures and the 3-D crustal model on top of it. The synthetic traveltime residuals are inverted for the upper-mantle structure, both with and without crustal corrections applied. We show for the Alpine region that neglecting crustal contribution in teleseismic tomography erroneously maps crustal anomalies into the upper mantle. The proper crustal correction of teleseismic traveltimes for any source–receiver pair significantly improves the resolution of upper-mantle structure in teleseismic tomography, in particular with densely distributed high-quality traveltime data.

2 3-D ALPINE CRUSTAL MODEL

2.1 Seismic data and model components

The Alps have been probed by various geophysical methods and a wealth of data have been obtained and interpreted to image the seismic structure of the crust and uppermost mantle at various scales (see e.g. Kissling 1993, for a review and references). From the published interpretations we choose structures that significantly affect seismic waves and produce characteristic phases in the traveltime–distance diagram, namely: the Moho topography, large and deep sedimentary basins, and the high-velocity Ivrea body. In comparison with these first-order structures, other intracrustal structures, such as variations in thickness of thin low-velocity layers or the topography of the boundary between the upper and the lower crust, only cause second-order effects (Waldhauser 1996) and are, therefore, not included in the 3-D model.

The crustal thickness for the model area is taken from Waldhauser *et al.* (1998), who modelled the simplest geometrical configuration of the crust–mantle boundary that is consistent with published seismic reflection and refraction data and corresponding error estimates of over 250 profiles across the Alpine region (Fig. 1). We have slightly extended this model to the south, west and east by including additional refraction data from Miller & Gebrande (1976), Stössenreuther (1982), Mechie *et al.* (1983) and Zeyen *et al.* (1997). The Moho topography beneath northern Italy and the Adriatic Sea, where no seismic profile data are available, is modelled to fit the structure proposed by Bigi *et al.* (1983). The Moho topography varies strongly in depth between 20 and 60 km, and shows two offsets that divide the interface into a European (M^E), an Adriatic (M^A) and a Ligurian Moho (M^L). The dominantly ENE–WSW-oriented offset below the Insubric Line (IL) in the north and the offset below the northern Apennines in the south indicate a southward subduction of the European lower crust under the shallower, north-dipping Adriatic Moho and a southward subduction of the Adriatic lower crust beneath the Ligurian Moho. The Adriatic Moho, while sandwiched between the European Moho in the north and the shallower Ligurian Moho in the south, is up-doming beneath the northern Po Plain (at about 45.5°N latitude and 10°E longitude in Fig. 1b).

Two sedimentary basins, the Molasse basin and the Po basin, domi nate the near-surface structure in the Alpine region. Fig. 2 shows the discretization of the near-surface information by defining polygons of constant sediment thickness and with specific *P*-wave velocities from top to bottom. The discretization introduces 2 km depth steps throughout the basin. The Molasse basin, running parallel to the Alpine strike in the north, thickens from NW towards SE from 0 km to about 5 km (Fig. 2), where it is overthrust by the Helvetic Nappes (not shown). Seismic velocities range from 3.7 to 4.4 km s^{-1} at the surface to 4.6–5.0 km s^{-1} at the bottom of the basin as obtained by controlled source seismic profiling (Lohr 1978; Zeis *et al.* 1990; Ye *et al.* 1995). The Quaternary and Tertiary sediments of the Po basin are sandwiched between the Alps and the northern Apennines

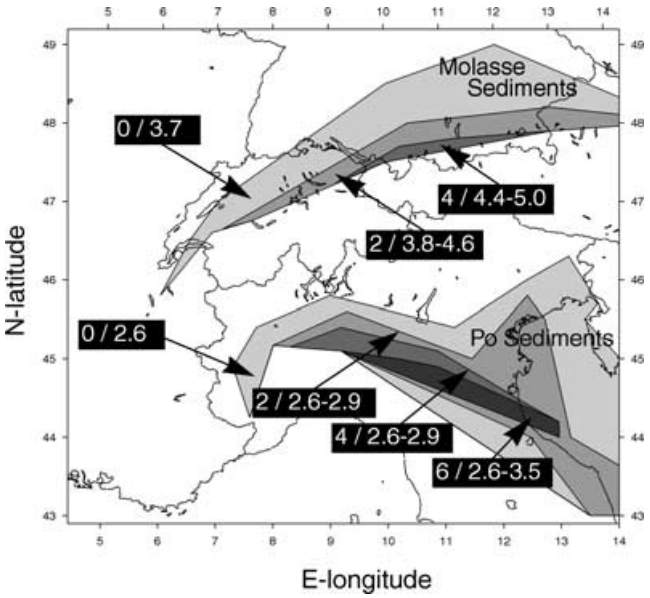

Figure 2. Molasse and Po plain near-surface sedimentary basin information, discretized by polygones. Numbers indicate sediment thickness (depth to top of basement in km) and *P* velocities in km s^{-1} at the surface and the base of the basins. Grey shades indicate sediment thickness.

(Pieri & Croppi 1981). The sediments thicken from 0 km at the northern margin to about 6 km in the south (Bigi *et al.* 1983; Cassano *et al.* 1986; Buness 1992) below the Apennine front. A velocity of 2.6 km s^{-1} at the surface of the sediment basins is derived along the European Geotraverse (EGT) (Blundell *et al.* 1992) and is extrapolated throughout the entire Po Basin. A *P* velocity of 2.9 km s^{-1} is used for the base of the Quaternary and upper Pliocene layers, and 3.5 km s^{-1} for the lower Pliocene (Buness 1992).

The Ivrea body is a structure of high density, high seismic velocity and high magnetic susceptibility located on the inner side of the western Alpine arc (Ménard & Thouvenot 1984). Solarino *et al.* (1997) derived a 3-D image of the western part of the Po Plain and the inner arc of the Western Alps encompassing the Ivrea body using local earthquake tomography (see Fig. 1a for model location). Their seismic structure for the Ivrea body shows a strong positive velocity perturbation relative to the tomographic reference velocities, with an average *P*-wave velocity of about 7 km s^{-1}. The spatial location of this structure agrees with that inferred from gravity data (Klingelé *et al.* 1992).

2.2 Model parametrization and the resulting 3-D model

The computerized model construction procedure (Waldhauser 1996) uses as a basic structure a three-layered model with spatially varying layer boundaries, consisting of a near-surface layer (A), a main crustal layer including middle and lower crust (B) and an uppermost-mantle layer (C) (Fig. 3a). Two transition zones (TZ_1 and TZ_2), represented by velocity gradients between adjacent grid nodes, separate the layers from each other, with the first one (TZ_1) corresponding to the top of the basement and the second one (TZ_2) to the crust–mantle boundary. *P* velocities are interpolated linearly between evenly spaced nodes with 2 km spacing. The grid spacing is in accordance with the typical resolution of the available seismic *a priori* information (i.e. optimally 2 km for Moho thickness, Braile & Chiang 1986; Deichmann *et al.* 1986). The Cartesian 3-D grid consists of $421 \times 331 \times 36$ grid nodes (840 km west–east, 660 km south–north and 70 km depth extension, respectively), encompassing the Alps and the northern Apennines between 3° and 14°E longitude, and 43° and 49°N latitude (see Fig. 1a for location). We obtain Cartesian coordinates by transforming spherical coordinates using a short-distance conversion with the transformation origin at 46.5°N latitude and 9°E longitude. The model surface is at sea level.

To ensure that the velocity information is complete on a regular grid, we establish a background velocity structure that we

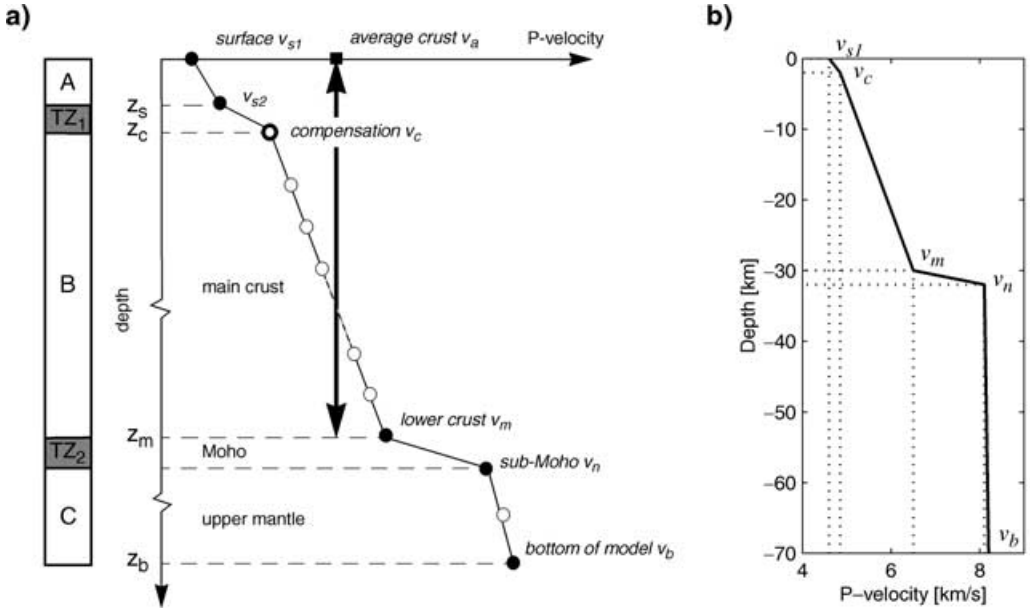

Figure 3. (a) Velocity–depth function of the three-layer (A, B, C) Alpine model with spatially varying layer boundaries (TZ_1, TZ_2). Solid dots represent velocity–depth information obtained either from seismic *a priori* information or from a reference model. The solid circle represents the compensation velocity calculated to derive adequate parametrization of the available seismic information. Light circles indicate interpolated values. See text for further explanation. (b) Reference velocity–depth function for the Alpine region.

subsequently update with the model components described above. The initial three-layer model (Fig. 3b) is based on a surface velocity (v_{s1}) of 4.6 km s^{-1}, a velocity v_m of 6.5 km s^{-1} at the base of the lower crust along the Moho interface of Waldhauser *et al.* (1998) and an average crustal velocity (v_a) of 6.1 km s^{-1}. The uppermost mantle is defined by a velocity v_n of 8.1 km s^{-1} below the Moho interface (at the base of TZ_2, Fig. 3a), gradually increasing with depth to a velocity v_b of 8.2 km s^{-1} at the base of the 3-D model at 70 km. These reference velocities are derived from averaging 2-D interpretations of seismic refraction data along the central segment of the EGT (Blundell *et al.* 1992) in the northern European foreland of the Alpine orogenic belt. The Moho interface (Fig. 1b) is discretized by piecewise-horizontal surfaces with discrete steps of 2 km.

Intracrustal velocities cannot be derived by simple interpolation between the surface velocity and the lower-crustal velocity since they would not necessarily fit the average crustal velocity. Following the general trend of the crust, the initial velocity–depth function is further characterized by a high velocity gradient in the uppermost crust and a much lower velocity gradient in the middle and lower crust. Thus, a new velocity parameter, the compensation velocity v_c (see Fig. 3), at the bottom of transition zone TZ_1 is used to retain the average crustal velocity without violating the velocities near the surface and at the bottom of the lower crust. The compensation velocity is obtained by relating the average crustal traveltime at normal incidence to the sum of average vertical traveltimes in each of the three zones A, TZ_1 and B, and is computed for every vertical grid line. In areas with no sediment coverage, TZ_1 represents the top layer of the model, with compensation velocities calculated at 2 km depth (Fig. 3b). The main crustal velocities are linearly interpolated between the compensation and the lower crustal velocity.

The sedimentary information (Fig. 2) is included by updating sediment velocities and basin depths (in steps of 2 km) at the corresponding nodes in the 3-D model. The compensation velocity is subsequently shifted to proper depths for every vertical grid line within the sedimentary basins, and velocities within the main crustal layer are adjusted by linear interpolation between the new compensation velocity and the lower crustal velocity. In a last step, absolute *P*-wave velocities associated with the Ivrea body are extracted from the tomographic model by Solarino *et al.* (1997) and attached to grid nodes at the corresponding locations within the main crustal layer (layer B in Fig. 3a).

Note that we use measured Moho depths from active seismic surveys, but rely on reference values for the velocity contrast across the discontinuity. This procedure is used because only in a few cases were the seismic profiles long enough for refracted waves to consistently sample the lower crust and the uppermost mantle (*Pn* phase) and to give reliable information on their velocity structure. However, we used the information from these few cases to determine the reference values. Except for areas where we have detailed crustal velocity structure from tomographic studies, the model contains average crustal velocity information. Such a parametrization is designed to quantify crustal effects on teleseismic wave fronts. For detailed tectonic interpretations, however, this generalized crustal model should not be used as it does not show the fine details of the intracrustal velocity structure.

The final 3-D model, shown in Fig. 4, represents the large-scale Alpine crustal structure, reflecting effects from the collision of the

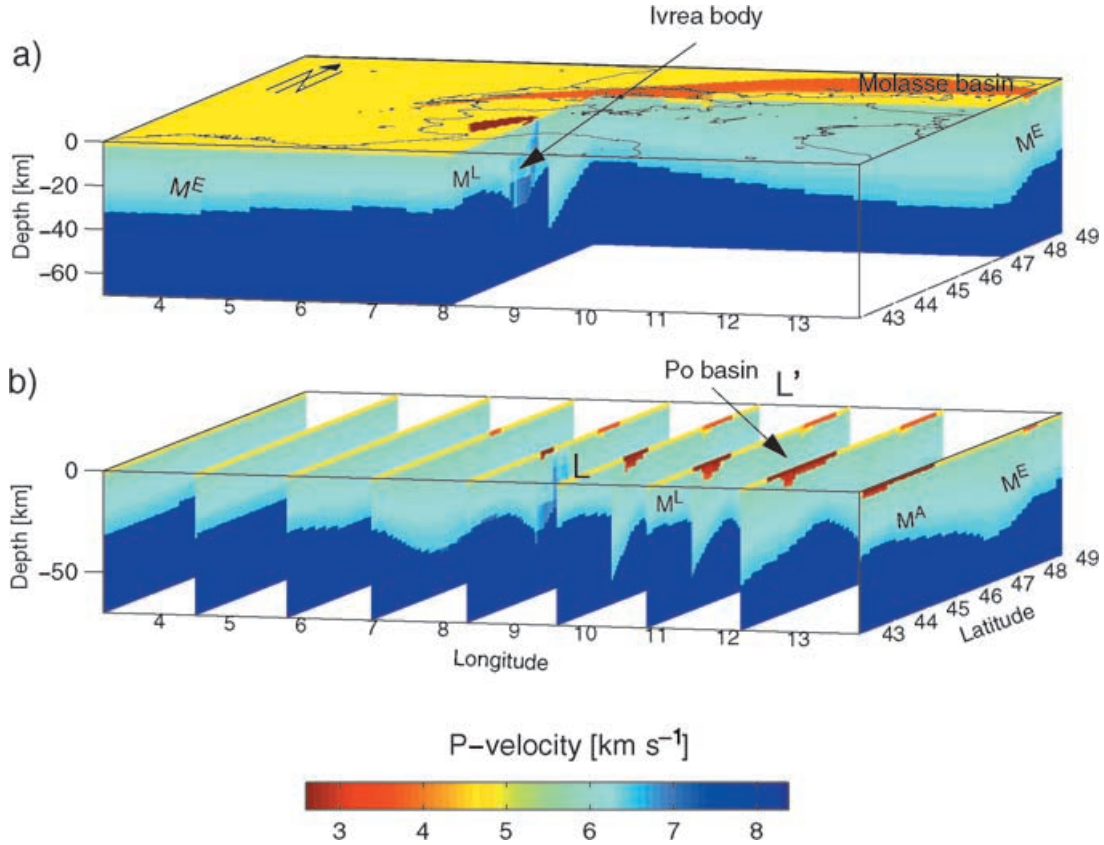

Figure 4. North–west perspective view of the final 3-D Alpine crustal *P*-velocity model, shown (a) in a cut-away display and (b) by south–north-oriented cross-sections. The Ligurian (M^L), the Adriatic (M^A), and the European (M^E) crustal blocks are visible as well as the sedimentary basins and the Ivrea body. The cross-section along L–L′ represents the velocity depth distribution along the European Geotraverse (EGT, Blundell *et al.* 1992).

African with the European plate (e.g. Schmid *et al.* 1996). In addition to the European, the Adriatic and the Ligurian crustal blocks, the velocity model includes the sedimentary basins and the Ivrea body. The steeply dipping Ivrea body is associated with the Adriatic crust, lying above the western tip of the Adriatic Moho and reaching the surface at the western end of the Po basin.

3 EFFECT OF 3-D CRUSTAL STRUCTURE IN TELESEISMIC TOMOGRAPHY

3.1 Crustal contribution to teleseismic traveltimes

Teleseismic traveltimes are calculated to the surface of the 3-D crustal model by coupling the reference whole-earth model IASP91 (Kennett & Engdahl 1991) to the finite-difference (FD) scheme of Vidale (1990) modified by Hole & Zelt (1995) (Fig. 5). The FD algorithm determines traveltimes from a given spherical wave front defined at the base of the 3-D velocity model using the IASP91 traveltime table to all points within the 3-D velocity grid, thus eliminating the need to search for a specific ray connecting source and receiver. The problem of the generally multi-valued nature of time fields is avoided by tracing only minimum arrival times. In contrast to single-ray methods, where traveltimes are obtained at specific points on the Earth's surface only (i.e. receiver sites), the wave front method yields the continuous time field of a teleseismic wave arriving at the Earth's surface.

Fig. 6 shows the effects of the 3-D crustal and uppermost mantle model on the traveltimes of a vertically incident planar wave front with zero-time at 70 km depth. It illustrates the relative traveltime delays (advances) across the model surface after subtracting a reference traveltime determined for the 1-D reference structure (see Fig. 3b). Relatively large traveltimes with respect to the reference correspond to positive residuals (shown in black), small traveltimes correspond to negative residuals (white). The Alpine sedimentary basins cause maximum delays of +1.4 s in the southern Po Plain and +0.2 s in the Molasse basin. These effects are enhanced by the topography of the crust–mantle boundary that causes large residuals along the strike of the thick European crust with residuals increasing towards the inner, deep arc of the Alpine orogen, reaching a maximum delay of about +1 s at the southern boundary of the European crust. Negative residuals reflecting the relatively thin crust are

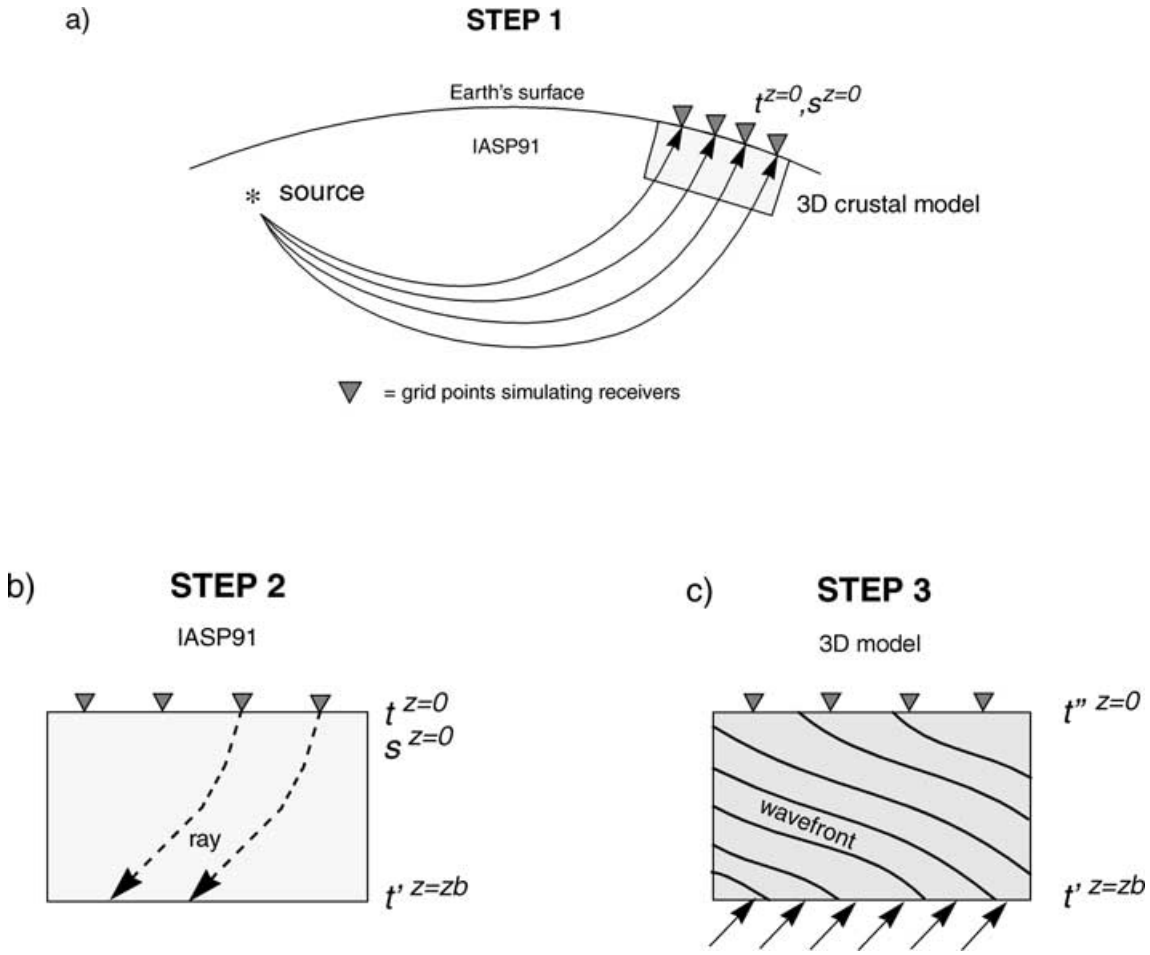

Figure 5. Three step procedure to solve the teleseismic forward problem using a standard Earth model (IASP91 Kennett & Engdahl 1991) and a 3-D crustal model. (a) Traveltimes t and slowness s are calculated for an arbitrary source at points on the Earth's surface in the local model using the reference whole-earth model IASP91 (Kennett & Engdahl 1991) (step 1). (b) To find the location where this slowness is appropriate at depth (base, z_b, of the 3-D model), the rays are traced back through the reference Earth model from the surface to the base of the local model using Snell's law (step 2). This yields entry points and corresponding traveltimes t' of the teleseismic signal into any 3-D structure on top of it. (c) In the third step the spherical wave front obtained in step 2 is propagated from the base of the local model to its surface. Traveltimes t'' through the heterogeneous 3-D velocity structure are calculated by means of finite differences (Vidale 1990; Hole & Zelt 1995).

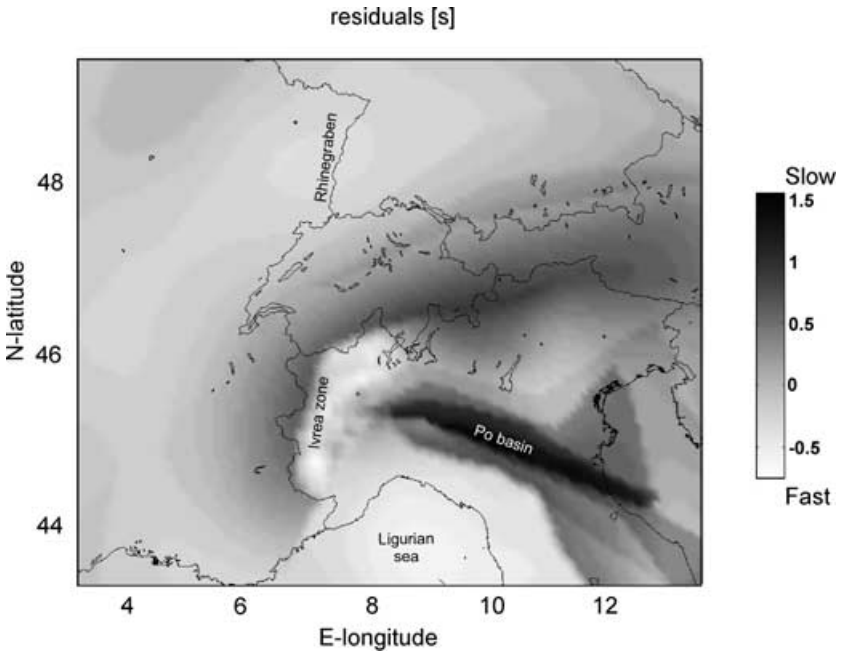

Figure 6. Traveltime residuals (s) for a vertically incident plane wave front between the 1-D reference model and the 3-D Alpine model. White represents fast regions, black slow regions.

observed under the Rhinegraben and the Ligurian Sea. The linear correlation between traveltime residuals and the crustal thickness in some areas is a result of the assumption of a constant average crustal velocity. Up to −0.7 s of early arrivals are observed at the western margin of the Po Plain above the Ivrea body.

Obviously, the effect of the 3-D crustal structure on teleseismic traveltimes depends not only on the local structure itself, but also on the backazimuth and epicentral distance of a specific event. Whereas the variation of teleseismic traveltime residuals owing to different epicentral distances is small because of the generally high angle of incidence of teleseismic wave fronts, the traveltime residual variation owing to different backazimuth can be large depending on the complexity of the local structure. For the Ivrea zone residual variations of up to 0.6 s are obtained. Fig. 7 demonstrates the effect of wave front distortion for an event located in the Kurile Islands by plotting traveltimes of first arrivals (solid lines) at the surface of the 3-D Alpine model. The overall pattern is similar to that of a wave front calculated for the 1-D reference model (dashed lines), but severe distortions of more than 1 s occur for the regions with deep and strongly heterogeneous velocity structure beneath the southern Alps, the Apennines and the Po Plain.

3.2 Inversion of synthetic traveltime residuals

The influence of the 3-D Alpine crustal structure in teleseismic tomography is investigated by inversion of synthetic traveltime residuals. The distribution of event sources is of great importance as the resolution of the inverted structure depends critically on the ray crossing from different azimuths and distances. Thus, we compute traveltimes using representative hypocentral parameters selected from a teleseismic data set recorded from 1998 to 2000 across the Alpine region during the tomography experiment Transalp (Lippitsch *et al.* 2001). 76 events with a total of 4285 observations were selected to represent a realistic ray coverage obtained during the 3 yr observational period. Fig. 8 shows the distribution of events and stations, including short-period and broad-band stations of several permanent seismic networks in the Alpine region (SED, Zürich; DISTER, Genova; SISMALP, Grenoble; EOST, Strasbourg; OGS, Trieste; GLBW, Freiburg, ZAMG, Wien; URGS/ARSO, Ljubljana; ING, Roma) and the temporary Transalp array.

First, we establish a synthetic upper-mantle model (Fig. 9a) mimicking two slab structures beneath the western Alps and the eastern Alps, respectively, which we aim to recover in the subsequent test inversions. The IASP91 model is used as background structure. A south-dipping structure is placed beneath the western Alps at depths between 120 and 350 km, featuring a 6 per cent velocity increase relative to the background model. The second anomaly represents an east-dipping structure beneath the eastern Alps at depths between 150 and 240 km with a velocity 3 per cent smaller than the background velocity. These features correspond approximately to anomalies previously documented by Spakman *et al.* (1993), among others, beneath the Alpine orogeny. We parametrize the model by a 3-D grid with 50 km horizontal and 30 km vertical grid spacing in areas with reasonable ray coverage, and even grid spacing of 50 km at the borders and the base of the model. The grid spacing is adapted to the distribution of stations and ray paths (Kissling *et al.* 2001) and guarantees uniform and fair resolution in most areas under study in the depth range 100–300 km.

The ray-bending method of Steck & Prothero (1991) is used to calculate traveltimes relative to a reference model for the synthetic mantle structure at the Alpine stations. The advantage of using relative traveltimes is that errors in source parameters and the velocity deviation from the IASP91 model for the path from the source through the mantle to the bottom of the local model are reduced. For each event only stations that actually recorded the event are used. A Gaussian error is added to the traveltimes to represent the picking uncertainty present in real data sets (±0.25 s for manually picked data; e.g. Arlitt 1999). The synthetic data set therefore represents realistic sampling.

Fig. 10(a) displays the calculated relative traveltime residuals (short: residuals) between the IASP91 model and the modified IASP91 model for an event located at 49.32° latitude and 155.63°

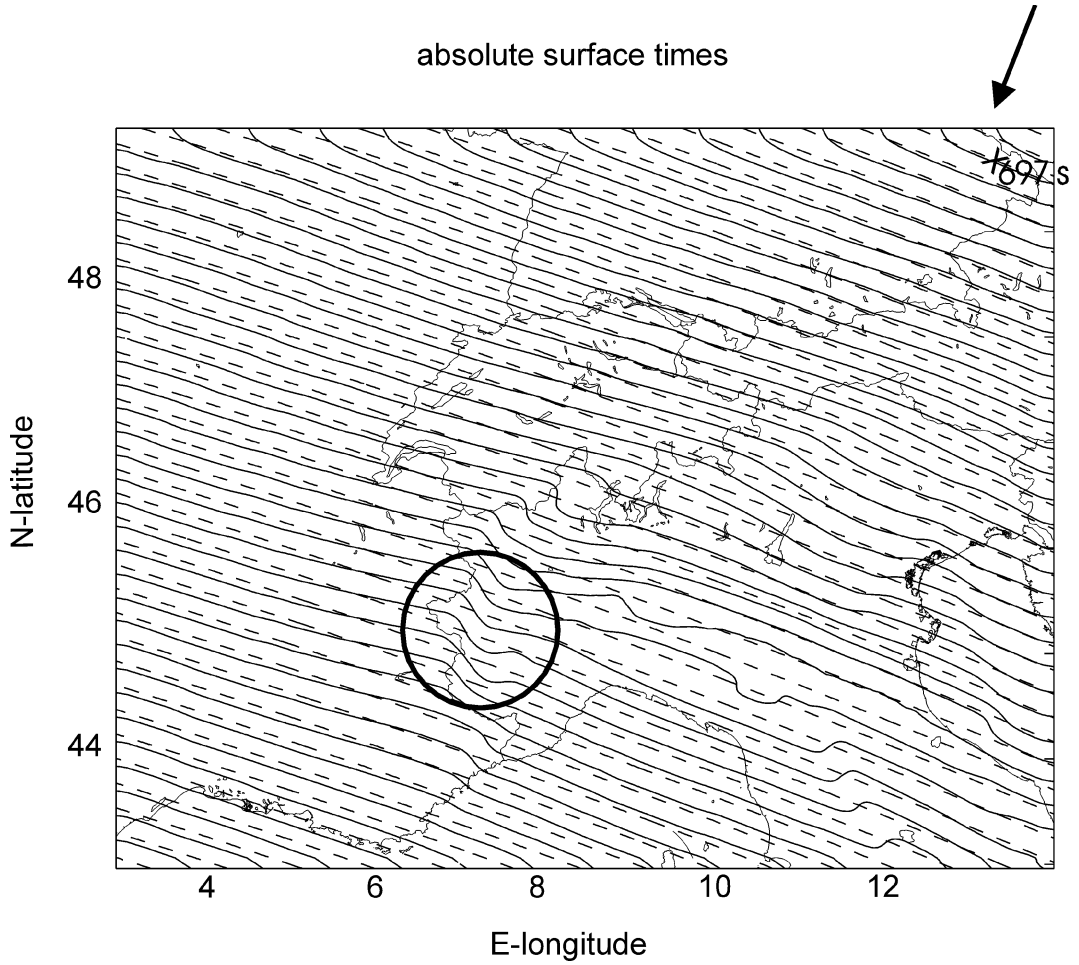

Figure 7. *P*-wave traveltimes (contoured at 1 s intervals) at the surface of the 3-D Alpine model (solid lines) and the 1-D reference model (dashed lines) (see Fig. 3b) calculated for an oblique incident spherical wave front of an event located in the Kurile Islands. Arrow represents azimuthal direction (27°). Angular distance is 82°. Number indicates absolute traveltime in s. Circle shows area with substantial wave front distortion.

longitude in the Kurile Islands (see Fig. 8a). The residuals indicate the effects from the two synthetic mantle structures (indicated by boxes) on the surface times at each station. Note the southwestward migration of the residuals owing to the oblique incidence of the wave front travelling through the deep seated anomalies. To investigate the effect of the 3-D Alpine crustal model we add the crustal contribution for each event/station configuration to the mantle residuals used above (Fig. 10b). This basically replaces the IASP91 1-D crust with our 3-D crustal model. In contrast to the 'crustal-corrected' residuals shown in Fig. 10(a), the uncorrected residuals in Fig. 10(b) show the superposition of the effects of both the two synthetic mantle structures (indicated by boxes) and the 3-D crustal structure, at each station. While the response of the high-velocity mantle anomaly (+6 per cent) is still visible in the data, crustal traveltime contributions completely mask the effect of the low-velocity mantle anomaly.

Our non-linear inversion technique is based on the formulation known as the ACH technique (Aki *et al.* 1977; Iyer & Hirahara 1993) with several significant modifications. The forward problem is solved by 3-D minimum traveltime ray tracing (Steck & Prothero 1991) using the simplex algorithm of Press *et al.* (1986). The non-linear inversion scheme iteratively inverts the residuals for velocity changes to an initial reference model, in our case IASP91. This approach has previously been applied to teleseismic data by Weiland *et al.* (1995) (among others).

The inversion scheme is first applied to the mantle residuals (Fig. 10a) to investigate the resolution capability of the data. Since no contribution from the crust is present in this data, nodes in the model grid that represent the crust were kept fixed during inversion. Results for this best-case scenario show adequate recovery of the amplitude and location of the upper-mantle structure (Fig. 9b). The two synthetic anomalies appear as two isolated bodies. While the dip of the high-velocity slab structure in the west is properly resolved, the dip of the low-velocity (small-amplitude) anomaly in the eastern part could not be recovered. The projection of negative anomalies into the northwestern part of the model is a result of inadequate ray coverage and ray crossing in this area. The tomographic image of the high-velocity anomaly shows typical smearing effects caused by the strongly non-uniform source distribution. The poorer recovery of the low-velocity structure is a result of the smaller amplitude in the velocity change (3 per cent).

Assuming that no *a priori* information concerning the crustal velocity distribution is available, we also invert the pure mantle residuals (Fig. 10a) for crustal nodes to account for potential anomalies in the crust. Because of the decrease in near-surface resolution resulting from the subvertical incidence of teleseismic waves, anomalies located in the mantle leak into the crust (Fig. 9c). The resulting tomographic image also shows the smearing of negative anomalies into the northwestern part of the model as seen in Fig. 9(b).

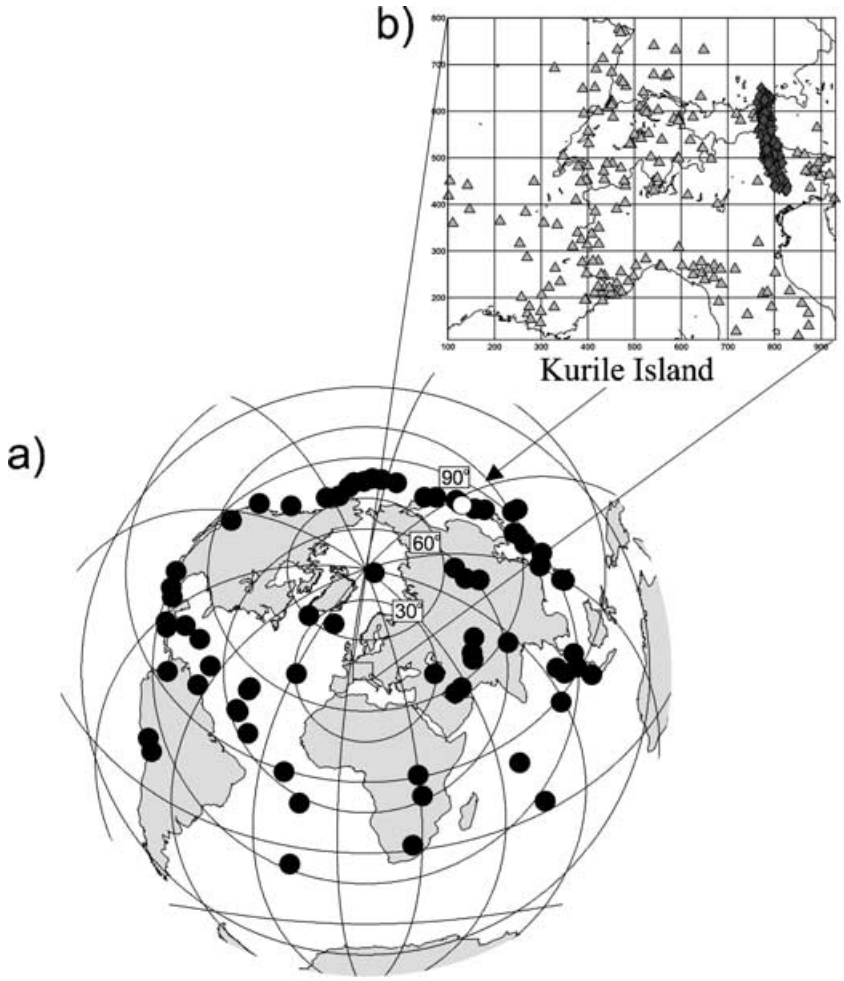

Figure 8. Distribution of (a) events and (b) stations for which teleseismic traveltimes are calculated. In (a) the projection is azimuthal equidistant with the study area as the projection pole. Open circle represents event used to generate Fig. 7. Triangles in (b) indicate permanent stations, diamonds are temporary stations in the Transalp array.

Nevertheless, the amplitudes of both and the dipping of the western high-velocity anomaly are properly resolved.

In the presence of strong crustal anomalies, the inversion of uncorrected residuals (shown in Fig. 10b) causes the crustal anomalies to leak into the upper mantle, even if the crustal nodes were kept floating during inversion (Fig. 9d). The recovered structure is strongly influenced by the crust in the upper layers. While the location of the high-velocity body and its dip are recovered, the low-velocity anomaly is completely masked. The anomaly pattern at 120 km depth can clearly be correlated with the crustal anomalies (see Fig. 6). Inversion of uncorrected residuals with the crustal nodes fixed (i.e. assuming that crustal effects are negligible) forces the crustal anomalies even deeper into the mantle (Fig. 9e). The artefacts observed in Fig. 9(d) are intensified but do not change the geometry significantly.

4 DISCUSSION AND CONCLUSION

Previous studies on teleseismic traveltime residuals were carried out along 2-D profiles (Baer 1980; Viel *et al.* 1991; Guyoton 1991) and/or used 1-D station corrections (Baer 1980; Babuska *et al.* 1990; Viel *et al.* 1991). Here we outlined a procedure to predict for any event the continuous seismic traveltime field across the greater Alpine region. Our approach allows the fast calculation of traveltime residuals at any given station location, properly corrected for the crustal structure that influences the traveltime of a specific event/station configuration. The underlying model for the Alpine crust (Fig. 4) is based on independent seismic data and represents the simplest model for fitting these data within their corresponding error bounds. The comparative use of both local tomographic information, which is sensitive to volumetric changes in velocity distribution, and seismic refraction and reflection information, which best images first-order discontinuities, allows one to integrate the structures significantly affecting teleseismic wave fronts in a 3-D model. The 3-D crustal model presented here is not a tectonic model, though, as it does not resolve detailed intracrustal structures important for tectonic interpretation. It may, however, serve as a reference for a wide range of other applications such as earthquake location, gravity calculation, geodynamic modelling and forecasting of shaking effects during large earthquakes, and builds a strong foundation for future refinements.

In this study we showed that the contribution of the 3-D crustal model to teleseismic traveltimes ranges between -0.7 and $+1.5$ s. The large residual variations are produced by the extreme variation in crustal thickness and the intracrustal velocity anomalies associated with the Ivrea body and the sedimentary basins. With a set of synthetic traveltimes, representing true teleseismic ray

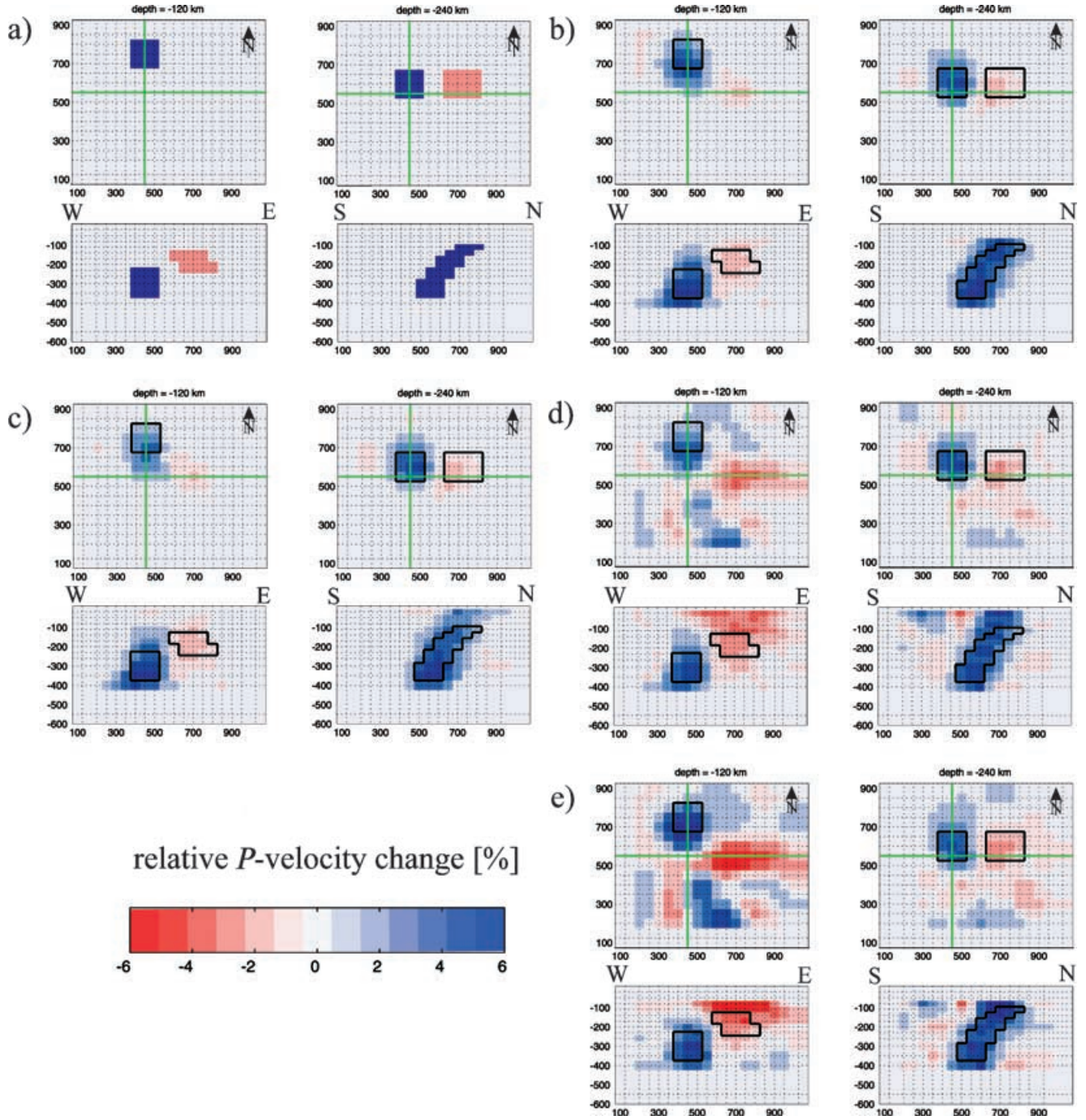

Figure 9. (a) Synthetic mantle model with velocity changes shown relative to the IASP91 reference structure. (b–e) Tomographic images after inversion of (b) corrected (mantle) residuals with crustal nodes fixed, (c) corrected residuals with crustal nodes floating, (d) uncorrected residuals with crustal nodes floating and (e) uncorrected residuals with crustal nodes fixed. Velocity changes are shown relative to the IASP91 reference structure. In each subfigure, top panels are depth slices at −120 and −240 km, and lower panels are cross-sections in W–E and S–N directions. Green lines in top panels indicate location of cross-sections shown in lower panels.

sampling for the current Alpine network and realistic pick errors, we further showed that the crustal anomalies are, if not corrected for, erroneously mapped into the upper mantle during inversion (Figs 9d and e). The artefacts reach depths of more than 200 km and show magnitudes of up to 5 per cent, significantly decreasing the resolution of the mantle structures we are tring to recover. These results, of course, depend critically on the correctness of the crustal model. While the model includes first-order structures, it does not account for second-order structures such as small-scale intracrustal velocity heterogeneities and discontinuities such as the interface between upper and lower crust. At present, the central Alps are the only area in the Alpine region where the lateral extension of the 2-D measured average crustal velocity can be modelled reliably by interpolation between closely spaced and networked profiles. Tests with locally updated average crustal velocities from these high-quality active source surveys revealed differences of less than 0.1 s in the

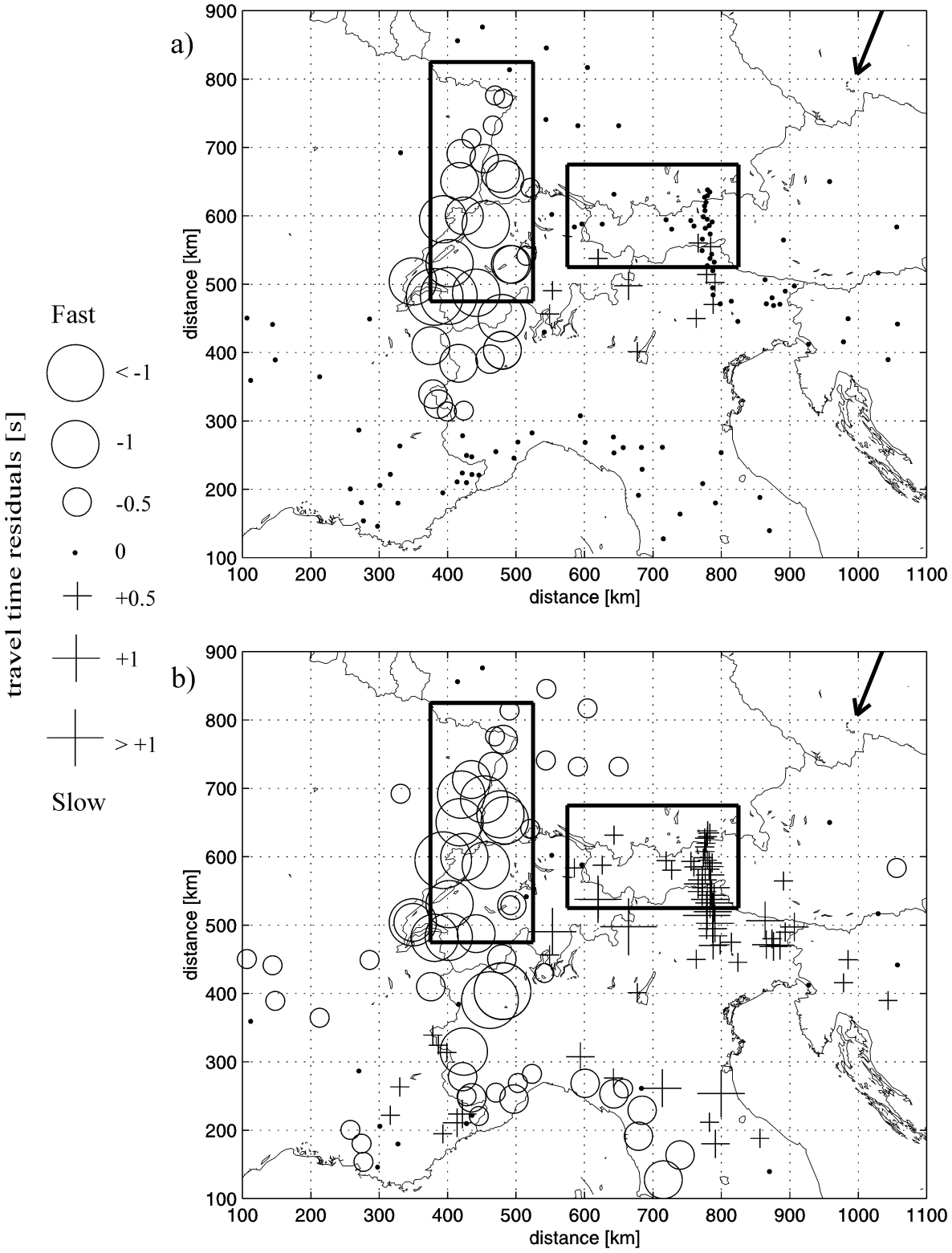

Figure 10. (a) Crustal-corrected (mantle) traveltime residuals. (b) Uncorrected residuals including the effect of the 3-D crustal structure. Circles represent fast, plus signs slow traveltimes relative to the IASP91 model. Size of the symbols scale with amplitude of the traveltime delay/advance. Boxes indicate the horizontal location of the synthetic anomalies in the mantle. Arrow indicates azimuth of incoming wave front.

resulting traveltime residuals, leading to second-order effects in the tomographic results. Future experiments are encouraged, however, to resolve the fine-scale velocity structure of the Alpine crust across the model region.

With azimuth- and distance-dependent residual variations of up to 0.6 s, static traveltime corrections in the Alpine region are grossly inadequate (see also Babuska *et al.* 1990; Kissling 1993). Ongoing studies (Lippitsch *et al.* 2001) use crustal-corrected residuals

of measured teleseismic traveltimes to invert for the upper-mantle structure in the Alpine region, with the aim to improve on earlier studies by Spakman *et al.* (1993). With *a priori* crustal correction and high-quality teleseismic data, we are able to decrease the cell size by a factor of at least 8 without loss of data resolution, hence obtaining a better recoverage of small-scale upper-mantle structures.

ACKNOWLEDGMENTS

We wish to thank Michael Korn, Uli Achauer, Rob van der Hilst, Tom Brocher and several anonymous reviewers for valuable comments on this and earlier versions of the manuscript. M. Baer, K. Stammler and J. Hole are thanked for supplying us with the seismic data analysis programs SNAP, and SeismicHandler and the FD traveltime code, respectively. We thank the following colleagues and services for providing us with teleseismic data: M. Baer, Swiss Seismological Service, ETH-Zürich; S. Solarino, Dipartimento di Scienze della Terra, University of Genova; F. Thouvenot, Observatoire de Grenoble, University of Grenoble; M. Granet and J. L. Biellmann, Ecole et Observatoire des Sciences de la Terre, Strasbourg; D. Slejko, A. Govoni and P.-L. Bragato, Osservatorio Geofisico Sperimentale, Trieste; W. Brüstle and S. Mellert, Seismological Service, Landesamt für Geologie Baden-Wuerttemberg, Freiburg; E. Schmedes, University of Munich; W. Lehnhardt and N. Horn, Zentralanstalt für Meterologie und Geodynamik, Wien; C. Chiarraba, ING, Roma; M. Zivcic and I. Cecic, URGS/ARSO, Ljubljana. Stipends from the Kanton of Basel and from ETH Zürich (FW) and support from the Swiss National Foundation (RL) is greatly acknowledged.

REFERENCES

Aki, K., Christoffersson, A. & Husebye, E.S., 1977. Determination of three-dimensional seismic structure of the lithosphere, *J. geophys. Res.,* **82,** 277–296.

Arlitt, R., 1999. Teleseismic body wave tomography across the Trans-European Suture Zone between Sweden and Denmark, *PhD thesis,* no 13501, ETH-Zürich, p. 109.

Babuska, V., Plomerova, J. & Granet, M., 1990. The deep lithosphere in the Alps: a model inferred from *P*-residuals, *Tectonophysics,* **1976,** 137–165.

Baer, M., 1980. Relative travel-time residuals for teleseismic events at the new Swiss seismic station network, *Ann. Géophys.,* **36,** 119–126.

Bigi, G., Castellarin, A., Coli, M., Dal Piaz, G.V., Sartori, R., Scandone, P. & Vai, G.B., 1983. Structural model of Italy, Sheet no 1, in *Progetto Finalizzato Geodinamica,* eds Bigi, G., Cosentino, D., Parotto, M., Sartori, R. & Scandone, P., *Cons. Naz. delle Ric.,* Rome, Italy.

Bijwaard, H. & Spakman, W., 2000. Non-linear global P-wave tomography by iterated linearized inversion, *J. geophys. Res.,* **141,** 71–82.

Blundell, D., Freeman, R. & Mueller, St. (eds.), 1992. *A Continent Revealed, the European Geotraverse,* Cambridge University Press, New York, p. 275.

Braile, L.W. & Chiang, C.S., 1986. The continental Mohorovicic discontinuity: results from near-vertical and wide-angle seismic reflection studies, in *Reflection Seismology; a Global Perspective,* Geodynamics Series, Vol. 13, pp. 257–272, eds Barazangi, M. & Brown, L., American Geophysical Union.

Buness, H., 1992. Krustale Kollisionsstrukturen an den Rändern der nordwestlichen Adriaplatte, *Berliner Geowissenschaftliche Abhandlungen,* Reihe B, 18, FU Berlin, p. 221.

Cassano, E., Aneli, L., Fichera, R. & Cappelli, V., 1986. Pianura Padana, interpretazione integrata di dati geofisici e geologici, *Con. Soc. Geol. Ital., Roma,* **73**, 36.

Cattaneo, M. & Eva, C., 1990. Propagation anomalies in Northwestern Italy by inversion of teleseismic residuals, *TerraNova,* **2,** 577–584.

Deichmann, N., Ansorge, J. & Mueller, St., 1986. Crustal structure of the Southern Alps beneath the intersection with the European Geotraverse, *Tectonophysics,* **126,** 57–83.

Engdahl, E.R., van der Hilst, R. & Buland, R., 1998. Global teleseismic Earthquake relocation with improved travel times and procedure for depth determination, *Bull. seism. Soc. Am.,* **88,** 722–743.

Guyoton, F., 1991. Sismicité et structure lithospherique des Alpes occidentales, *PhD thesis,* Observatoire de Grenoble et Institut de Recherches Interdisciplinaires de Géologie et de Méchanique, Univ. Joseph Fourier de Grenoble, p. 290.

Hole, J.A. & Zelt, B.C., 1995. 2-D finite-difference reflection traveltimes, *Geophys. J. Int.,* **121,** 427–434.

Iyer, H.M. & Hirahara, K. (eds.), 1993. *Seismic Tomography—Theory and Practice,* Chapman and Hall, London.

Kennett, B.L.N. & Engdahl, E.R., 1991. Travel times for global earthquake location and phase identification, *Geophys. J. Int.,* **105,** 429–465.

Kissling, E., 1993. Deep structure of the Alps—what do we really know?, *Phys. Earth planet. Inter.,* **79,** 87–112.

Kissling, E., Husen, S. & Haslinger, F., 2001. Model parametrization in seismic tomography: a choice of consequence for the solution quality, *Phys. Earth planet. Inter.,* **123,** 89–101.

Klingelé, E., Lahmeyer, B. & Freeman, R., 1992. EGT gravity anomaly map, central and southern segments, in *A Continent Revealed, the European Geotraverse,* eds Blundell, D., Freeman, R. & Mueller, St., Cambridge University Press, New York.

Lippitsch, R., Kissling, E. & Ansorge, J., 2001. Mapping the structure of the lithosphere-asthenosphere system under the Alpine Orogen with high-resolution teleseismic tomography (abstract), *EOS, Trans. Am. geophys. Un.,* **82**, Fall Meet. Suppl.

Lohr, J., 1978. Alpine stress documented by anomalous seismic velocities in the Molasse throug, in *Alps, Apennines, Hellenides,* pp. 69–71, eds Closs, H., Roeder, D. & Schmidt, K., Schweizerbart Verlag, Stuttgart, Germany.

Mechie, J., Prodehl, C. & Fuchs, K., 1983. The long-range seismic refraction experiment in the rhenish massiv, in *Plateau Uplift: the Rhenish Shield—a Case History,* pp. 260–275, ed. Fuchs, K., Springer-Verlag, Berlin.

Ménard, G. & Thouvenot, F., 1984. Ecailage de la lithosphère européenne sous les Alpes occidentales: arguments gravimétriques et sismiques liés à l'anomalie d'Ivrea, *Bull. Soc. Géol. France.,* **26,** 875–884.

Miller, H. & Gebrande, H., 1976. Crustal Structure in southerneast Bavaria derived from seismic refraction measurements by ray tracing methods, in *Explosion Seismology in Central Europe,* pp. 339–346, ed. Giese, P. *et al.*, Springer-Verlag, Berlin.

Mooney, W.D., Laske, G. & Masters, T.G., 1998. CRUST 5.1: A global crustal model at 5 × 5, *J. geophys. Res.,* **103,** 727–747.

Owens, T.J. & Zandt, G., 1997. Implications of crustal property variations for models of Tibetian plateau evolution, *Nature,* **187,** 37–43.

Pieri, M. & Croppi, G., 1981. Subsurface geological structure of the Po plain, Italy, CNR Progretto Finalizzato Geodinamico, Sottoprogretto 'Modello Structurale', *Publ.,* **414,** 1–13.

Poupinet, G., Thouvenot, F., Zolotov, E.E., Matte, Ph., Egorkin, A.V. & Rockitov, V.A., 1997. Teleseismic tomography across the middle Urals: lithopsheric trace and ancient continental collision, *Tectonophysics,* **276,** 19–33.

Press, W.H., Flannery, B.P., Teukolsky, S.A. & Vetterling, W.T., 1986. *Numerical Recipes: the Art of Scientific Computing,* Cambridge University Press, Cambridge.

Schmid, S.M., Pfiffner, O.A., Froitzheim, N., Schönborn, G. & Kissling, E., 1996. Geophysical–geological transect and tectonic evolution of the Swiss–Italian Alps, *Tectonics,* **15,** 1036–1064.

Solarino, S., Kissling, E., Sellami, S., Smriglio, G., Thouvenot, F., Granet, M., Bonjer, K.P. & Sleijko, D., 1997. Compilation of a recent seismicity database of the greater Alpine region from several seismological networks and preliminary 3-D tomographic results, *Ann. Geofis.,* **11,** 161–174.

Spakman, W., van der Lee, S. & van der Hilst, R., 1993. Travel-time tomography of the European–Mediterranean mantle down to 1400 km, *Phys. Earth planet. Inter.,* **79,** 3–74.

Steck, L.K. & Prothero, W.A., 1991. A 3D raytracer for teleseismic body wave arrival times, *Bull. seism. Soc. Am.,* **83,** 1332–1339.

Stössenreuther, U., 1982. Die Struktur der Erdkruste am Südwest-Rand der Böhmischen Masse, abgeleitet aus refraktionsseismischen Messungen der Jahre 1970 und 1978/1979, *PhD thesis,* Universitat München.

Van der Hilst, R.D., Widiyantoro, S. & Engdahl, E.R., 1997. Evidence for deep mantle circulation from global tomography, *Nature,* **386,** 578–584.

Vidale, J.E., 1990. Finite-difference calculation of traveltimes in three dimensions, *Geophysics,* **55,** 521–526.

Viel, L., Berckhemer, H. & Mueller, St., 1991. Some structural features of the Alpine lithospheric root, *Tectonophysics,* **195,** 421–436.

Waldhauser, F., 1996. A parametrized three-dimensional Alpine crustal model and its application to teleseismic wavefront scattering, *PhD thesis,* no 11940, ETH-Zürich, p. 173.

Waldhauser, F., Kissling, E., Ansorge, J. & Mueller, St., 1998. Three-dimensional interface modelling with two-dimensional seismic data: the Alpine crust–mantle boundary, *Geophys. J. Int.,* **135,** 264–278.

Weber, M., 1994. Traveltime and amplitude anomalies at the seismic broadband array GRF, *Geophys. J. Int.,* **118,** 57–74.

Weiland, C.M., Steck., L.K., Dawson, P.B. & Korneev, V.A., 1995. Nonlinear teleseismic tomography at Long Valley caldera using three-dimensional minimum travel time ray tracing, *J. geophys. Res.,* **100,** 20 379–20 390.

Ye, S., Ansorge, J., Kissling, E. & Mueller, St., 1995. Crustal structure beneath the eastern Swiss Alps derived from seismic refraction data, *Tectonophysics,* **242,** 199–221.

Zeis, St., Gajewski, D. & Prodehl, K., 1990. Crustal structure of southern Germany from seismic refraction data, *Tectonophysics,* **176,** 59–86.

Zeyen, H., Novak, O., Landes, M., Prodehl, C., Driad, L. & Hirn, A., 1997. Refraction-seismic investigations in the northern Massif Central (France), *Tectonophysics,* **275,** 9–117.